Analysis and prediction of the diameter and orientation of AC electrospun nanofibers by response surface methodology

He H., Wang Y., Farkas B., Nagy Zs. K., Molnár K.

Materials and Design 194 (2020) 108902

Contents lists available at ScienceDirect

Materials and Design

journal homepage: www.elsevier.com/locate/matdes

Analysis and prediction of the diameter and orientation of AC electrospun nanofibers by response surface methodology

Haijun He [a], Yimeng Wang [a], Balazs Farkas [b], Zsombor Kristof Nagy [b], Kolos Molnar [a,c,*]

[a] Department of Polymer Engineering, Faculty of Mechanical Engineering, Budapest University of Technology and Economics, Műegyetem rkp. 3-9, H-1111 Budapest, Hungary
[b] Department of Organic Chemistry and Technology, Faculty of Chemical Engineering, Budapest University of Technology and Economics, Műegyetem rkp. 3-9, H-1111 Budapest, Hungary
[c] MTA–BME Research Group for Composite Science and Technology, Műegyetem rkp. 3, H-1111 Budapest, Hungary

HIGHLIGHTS

- We studied the parameter effects on the AC electrospun nanofiber diameter and orientation with response surface methodology.
- We used the Box-Behnken design model to predict the nanofiber diameter and orientation.
- Concentration and collection speed had similar influences on fiber diameter and orientation in AC and DC electrospinning.

GRAPHICAL ABSTRACT

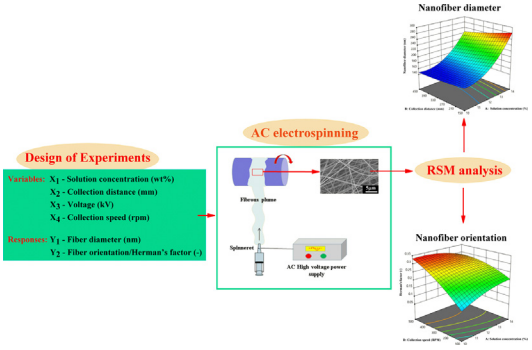

ARTICLE INFO

Article history:
Received 26 April 2020
Received in revised form 13 June 2020
Accepted 18 June 2020
Available online 25 June 2020

Keywords:
AC electrospinning
Response surface methodology
Box-Behnken design model
Nanofiber diameter and orientation

ABSTRACT

In this study, we analyzed the influence of process parameters on the diameter and orientation of nanofibers electrospun with alternating current (AC), using surface response methodology. The design of experiment was adopted with four main process parameters: solution concentration, collection distance, voltage and collection speed. The morphology of nanofibers was examined with a scanning electron microscope. Nanofiber orientation was characterized by the fast Fourier transform method. We used the Box-Behnken design model to predict the diameter and orientation of the nanofibers, and the results showed good agreement with the measured results. The results also indicated that solution concentration and collection speed have a similar influence on fiber diameter and orientation, as in the case of direct current electrospinning. Furthermore, in this study, we optimized the process parameters to generate thinner nanofibers with better alignment, and it also can be used as a reference to make nanofiber yarns with AC electrospinning.

1. Introduction

Electrospinning has been known for decades as an effective technology to produce nanofibers due to its simplicity and low cost. However, low nanofiber throughput of single-needle electrospinning (0.01–1 g/h) [1] and the simple structure of nanofibers hinder the development of electrospinning and nanofibers. Therefore, researchers have been focusing on the development of complex nanostructure and large-scale

* Corresponding author at: Department of Polymer Engineering, Faculty of Mechanical Engineering, Budapest University of Technology and Economics, Műegyetem rkp. 3-9, H-1111 Budapest, Hungary.
E-mail address: molnar@pt.bme.hu (K. Molnar).

https://doi.org/10.1016/j.matdes.2020.108902

production recently. Lots of efforts have been devoted to fabricating electrospun nanofibers with complex structure, such as core-sheath [2], Janus [3], tri-layer core-shell [4,5], hollow with multiple channels [6] with some novel electrospinning methods, such as using pulsed voltage [7] and melt electrospinning writing [8]. Moreover, much research has been devoted to increasing nanofiber throughput.

Today, a number of companies can mass-produce nanofibers for commercial products [9,10]. Researchers have been experimenting with various techniques for large-scale nanofiber production, such as multiple hole electrospinning [11], air-blowing assisted electrospinning [12] and needleless electrospinning [13]. Compared with needleless electrospinning, interference between the multiple jets and complicated device design are disadvantages of multiple-holes and air-blowing assisted electrospinning. Initially, needleless electrospinning was developed to increase productivity by generating multiple jets from a free liquid surface. For example, bubble electrospinning was introduced with the enhanced productivity of 2.35 g/h [13]. Later, some alternative spinneret geometries were reported to increase nanofiber productivity, such as ball (3.1 g/h) [14], cylinder (8.6 g/h) [15], rotary disk (6.2 g/h) [16], rotary wire (0.05 g/h/wire) [17] and spiral coil (2.94–9.42 g/h) [18]. The limitation of these needleless electrospinning methods was the rapid evaporation of solvent from the open liquid surface. To further reduce solvent evaporation from an open liquid surface, some modified needleless electrospinning methods were developed. In all these methods reported in the literature, multiple jets were generated from a tiny slit/slot [19–22]. Among them, corona electrospinning developed by Molnar and Nagy [21] achieved a significant improvement in nanofiber productivity (60 g/h) compared to single-needle electrospinning. Most recently, He et al. [23] designed a new spinneret with a textile yarn to address the problems existing in Nanospider with a wire spinneret. When the carriage is sliding to supply solution on the wire spinneret, it can occasionally interrupt the spinning process during its movement. In He's new design, a flexible textile yarn was used as the spinneret, and it had a productivity around 1.17 g/h. To enhance the spinnability of the highly viscous polymer solution, He et al. [24,25] modified the corona electrospinning setup by applying shearing force to shear-thin the polymer solution during the spinning process. As a result, the viscosity of the solution was reduced, which made it easier for multiple jets to form, and productivity reached 1.5 g/h with a 50 mm diameter spinneret.

In all the above-mentioned electrospinning methods, a static direct current (DC) high voltage was used to form an electrical field between the spinneret and the collector. In recent years, it was found that an alternating current (AC) also can be used to make electrospun nanofibers [26–29]. In comparison with DC electrospinning, AC electrospinning has some advantages. Firstly, multiple jets can be formed on the droplet surface during AC electrospinning, while there is one single jet formed on the droplet surface during DC electrospinning. Therefore, AC electrospinning has a higher nanofiber throughput, which is up to 20 times more with the same spinneret than in the case of DC electrospinning [30]. Besides, the resulting fibrous plume generated from AC electrospinning does not carry too many charges due to the high AC voltage, so a grounded conductive collector does not have to be used. The movements of the plume are mainly influenced by the electric wind instead of the attraction from the collector [28]. Whereas in DC electrospinning, the grounded collector plays a crucial role in the fiber formation process and affects the resulting structure of the collected fibers. Most importantly, the self-bundling of the fibrous plume from AC electrospinning makes it facilitate twisting the fibers into a yarn [26] because the rapid change between the positive and negative charges results in the sticking behavior of the nanofibers. However, little attention has been paid to the effect of processing parameters on fiber diameter with AC electrospinning. As for the orientation of AC electrospun nanofiber, we could not find any studies on it.

The object of this work is to predict fiber diameter and orientation with domain processing parameters using response surface methodology (RSM) and Box-Behnken design (BBD). Four processing parameters (solution concentration, voltage, collection distance, and rotation speed) were regarded as critical parameters in our experiments; we included them in BBD models to determine fiber diameter and orientation. RSM method has been used to study the effects of single factors and interactions of factors on the responses with the mathematical model in DC electrospinning [31–37]. With the elaborated models, we evaluated the significance of the effects of the parameters on fiber diameter and orientation, and optimized the process parameters for desirable fiber diameter and orientation. Also, AC electrospinning was compared to DC electrospinning. In this study, we used polyacrylonitrile (PAN) for electrospinning, because it is one of the most widely used polymers in electrospinning due to its good spinnability and the excellent mechanical properties of PAN nanofibers [38].

2. Experimental

2.1. Materials

We prepared PAN (M_w = 90,000 g/mol, Hangzhou Bay Acrylic Fiber Co., Ltd., China) solutions (10, 12 and 14 wt%) by dissolving PAN powder into *N*, *N*-dimethylformamide (DMF, 99%) and stirring it on a hot plate at 70 °C for 10 h until the solutions became homogenous. DMF was purchased from Azur Chemicals (Hungary).

2.2. AC electrospinning

AC electrospinning has basically the same elements as DC electrospinning, except for the high voltage power supply. The AC voltage was generated with an FME-24 voltage transformer (24,000 V/100 V ratio) (Transzvill Ltd., Budapest, Hungary). The effective voltage applied to the nozzle (inner and outer diameter is 1 mm and 2 mm, respectively) is the root mean square (RMS) voltage of the 50 Hz sinusoidal wave. The output voltage was adjusted manually with another variable transformer connected to the input of the high-voltage transformer. When the polymer solution was pumped through the nozzle with a syringe pump (Aitecs SEP-10S Plus, Lithuania), multiple jets were ejected from the nozzle. As the charges change over time, the overall charge of the polymer jet is negligible. Therefore, the polymer jets do not repulse one another, and they do not diverge. In the electrospinning process, there is a fibrous plume [26] consisting of multiple jets, as depicted in Fig. 1.

The fibrous plume flew up because of the electric wind. The nanofibers were then winded onto the rotating drum collector with a diameter of 70 mm, which was mounted vertically over the nozzle at a distance between 150 mm and 450 mm. The rotational speed of the drum collector was varied between 100 rpm and 500 rpm. After the electrospinning process, the collected nanofiber membrane was peeled off the drum for measurement. All the experiments were carried out with a constant flow rate of 10 ml/h. Relative humidity and ambient temperature during the experiments were 35 ± 2% and 25 ± 2 °C, respectively.

2.3. Characterization

The morphology of nanofibers was investigated with a scanning electron microscope (SEM) (JEOL 6380 LA, Japan). Before the SEM analysis, nanofibers were coated with a gold-palladium (Au/Pd) alloy for 30 s. We used the ImageJ software to analyze the fiber diameters by measuring 100 fibers chosen randomly from a sample. The fast Fourier transform (FFT) analysis function of ImageJ was used to determine fiber orientations.

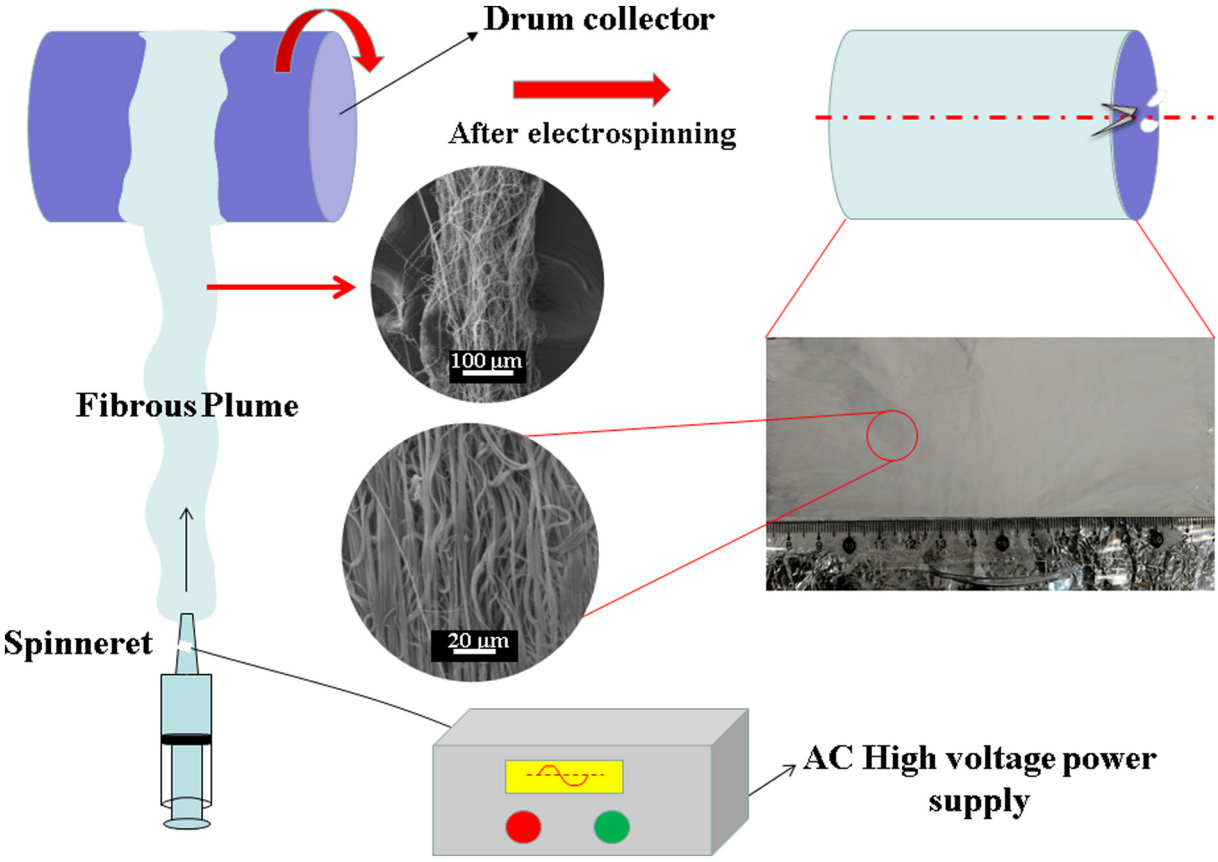

Fig. 1. Schematics of the fabrication and collection of nanofibers with AC electrospinning.

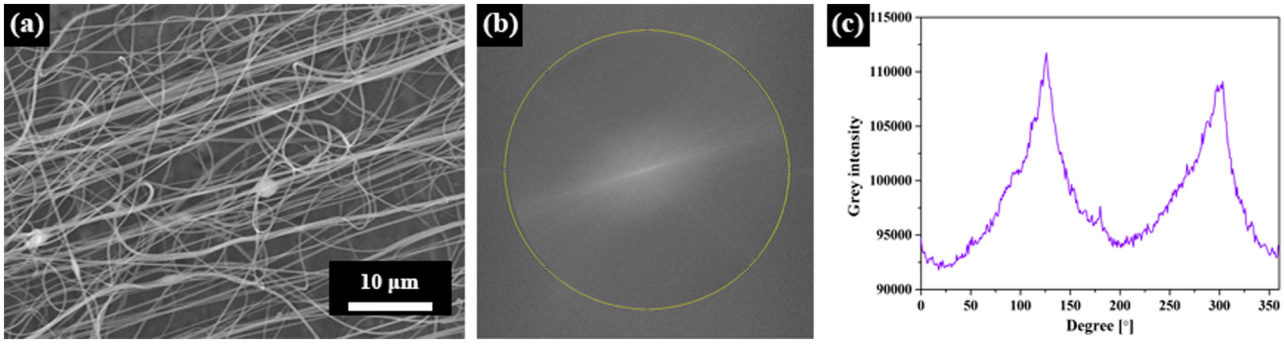

Fig. 2. FFT conversion from a SEM image to the intensity spectrum: (a) SEM image of nanofiber; (b) FFT frequency spectrogram; (c) grey intensity spectrum.

2.4. Fiber orientation analysis with FFT

We performed FFT analysis for SEM images (see Fig. 2a) with a magnification of 2000× to evaluate the fiber alignments. The FFT function converts the information contained in the optical data image from a "real" domain into a mathematically defined "frequency" domain [39]. As the first step of the FFT analysis, the FFT frequency spectrogram was obtained, as shown in Fig. 2b. Then the function of the Oval Profile (a plugin supported by ImageJ) was used to sum up the intensity in the radial direction between 0 and 360° on the selected projection area. The obtained intensity spectrum is shown in Fig. 2c. For all the obtained spectra, we observed the peaks related to the main fiber directions.

To quantify the orientation of the samples, we used Herman's factor [40] to determine the orientation degree of the fibers. It can be calculated with Eqs. (1) and (2):

$$f = \frac{3\mathrm{b}\cos^2\phi\mathrm{N} - 1}{2} \tag{1}$$

$$\mathrm{b}\cos^2\phi\mathrm{N} = \frac{\sum_{\phi=0^\circ}^{90^\circ} I(\phi)\sin\phi\cos^2\phi}{\sum_{\phi=0^\circ}^{90^\circ} I(\phi)\sin\phi} \tag{2}$$

where ϕ is the azimuthal angle, and $I(\phi)$ is the grey intensity along the angle ϕ. If all the fibers are ideally oriented along the reference direction, $\phi = 0°$ and $f = 1$. On the contrary, if all the fibers are perpendicular to the reference direction, $\phi = 90°$ and $f = -0.5$. In the case of random orientation, f equals to 0.

Table 1
Box-Behnken Design involving four parameters with three levels.

Sample no.	Solution concentration (%)	Collecting distance (mm)	Voltage (kV)	Rotation speed (rpm)
1	10	150	20	300
2	14	150	20	300
3	10	450	20	300
4	14	450	20	300
5	12	300	15	100
6	12	300	25	100
7	12	300	15	500
8	12	300	25	500
9	10	300	20	100
10	14	300	20	100
11	10	300	20	500
12	14	300	20	500
13	12	150	15	300
14	12	450	15	300
15	12	150	25	300
16	12	450	25	300
17	10	300	15	300
18	14	300	15	300
19	10	300	25	300
20	14	300	25	300
21	12	150	20	100
22	12	450	20	100
23	12	150	20	500
24	12	450	20	500
25	12	300	20	300
26	12	300	20	300
27	12	300	20	300
28	12	300	20	300
29	12	300	20	300

2.5. Design of experiments

To investigate the effect of multiple processing parameters on nanofiber diameter and orientation, we used the Box-Behnken design. In this study, there are mainly four processing parameters: solution concentration, collecting distance, voltage, and collector drum rotation speed, all with three levels. The parameter ranges (*i.e.*, solution concentration: 10%, 12%, 14%, collecting distance: 150 mm, 300 mm 450 mm, voltage: 15 kV, 20 kV, 25 kV, rotation speed: 100 rpm, 300 rpm, 500 rpm) were obtained based on preliminary experiments. The experimental design is shown in Table 1.

3. Results and discussion

3.1. Correlation between processing parameters and fiber diameter

The maximum and minimum of fiber diameter were obtained from samples 2 and 19, which gave an average fiber diameter of 279.6 ± 40.3 nm and 149.0 ± 32.3 nm, respectively (For the detailed results, see the supplement, Table S1). The SEM images and diameter distribution of fibers from the two samples are shown in Fig. 3. There were a few beaded fibers in sample 19 due to the smallest solution concentration and the highest voltage. In contrast, the fibers from sample 2 were straighter, and the average fiber diameter was larger.

Table 2 shows the results obtained using ANOVA, such as the *p*-value, coefficient of determination (R^2), standard deviation (*SD*), adjusted R^2, and predicted R^2. The importance of each parameter was determined by the *p*-values. The factors are indicated as the most significant factors when their *p*-values are <0.05. Therefore, based on the results summarized in Table 2, solution concentration, collection distance, and squared solution concentration show a substantial effect on the mean fiber diameter since their *p*-values are <0.05. The *p*-value for the model is <0.0001, which suggests that the model is considered statistically significant. Moreover, the value of R^2 is 97.45% for the model, indicating that 2.55% of all the variables are out of the regression model. Therefore, it is proved that the model is in good agreement with our experimental results. Also, the high value (94.90%) of adjusted R^2 indicates that the model has considerable significance. The model obtained from the ANOVA analysis can be written as shown in Eq. (3).

$$\begin{aligned} Y_1\ (\text{average fiber diameter}) = {} & 1214.08 - 179.627X_1 \\ & + 0.329281X_2 - 15.2553X_3 \\ & - 0.00131937X_4 - 0.02195X_1X_2 \\ & + 0.56085X_1X_3 - 0.0015875X_1X_4 \\ & + 0.00768567X_2X_3 \\ & + 0.00008171X_2X_4 - 0.0027275X_3X_4 \\ & + 8.3456{X_1}^2 + 0.000118063{X_2}^2 \\ & + 0.275892{X_3}^2 + 0.000157226{X_4}^2 \end{aligned} \quad (3)$$

The equation shows the relationship between the processing parameters and fiber diameter. To simplify and further analyze the experimental results, we created a reduced model that only includes the significant terms, to describe the variation in fiber diameter by the linear terms (X_1, X_2) and second-order term (X_1^2) as other terms are not significant. Fig. 4 presents that the predicted fiber diameters are in good agreement with the actual fiber diameter, which suggests that the model can be considered accurate.

The individual effect of solution concentration, collection distance, voltage, and collection speed on nanofiber diameter is shown in Fig. 5. Solution concentration has the most significant effect among the four processing parameters because its plot has the steepest slope. Nanofiber diameter increases with increasing solution concentration. It is because a more concentrated solution has higher viscosity due to the more entanglements among the polymer chains, which means higher viscous resistance against stretching forces [24]. Eventually, thicker nanofibers are obtained in that case. Besides, we also found that the effect plot of collection distance is more monotonous, compared to those of the voltage and collection speed. With increasing collection distance, fiber diameter slightly decreased. The reason is that when collection distance is too small, the rotating collector cannot provide sufficient stretching time before the nanofibers are winded up. Otherwise, the nanofibers can be stretched sufficiently with longer collection distance, resulting in smaller fiber diameter. Compared to the two parameters mentioned above (solution concentration and collection distance), voltage and collection speed only have a minor effect on average fiber diameter. If the voltage is too low, the electrical force may not be enough to stretch the polymer solution into fine nanofibers. When the voltage is too high, greater stretching can break the continuous polymer jets, leading to a small increase in nanofiber diameter. Collection speed has a similar effect on nanofiber diameter as voltage. Slower collection speed is not adequate for stretching, while faster speed results in polymer jets breaking. Therefore, the finest nanofibers are only produced at the right voltage and collection speed. In the literature, besides the discussed processing parameters that influence nanofiber diameter, some other parameters characterizing the droplet and jets, have also been investigated for control of nanofiber diameter for DC electrospinning, such as the height of the Taylor cone, the length of the straight fluid jet, and the angle of the Taylor cone [41–43].

Fig. 6 shows the effect of the interaction of different parameters with 3D response surface plots, which show the dependence of fiber diameter on the two independent parameters in the experimental range of the parameters. It can be seen in Fig. 6a, b, and c that solution concentration plays a dominant role in determining fiber diameter. Fiber diameter increases significantly from 10% to 14%. Nanofiber diameter does not change significantly with various collection distances, voltages, and collection speeds at any solution concentration in the range of 10%–14%. Fig. 6d, e and f show the interaction of other parameters except for solution concentration with 3D surface plots. The plot surfaces are flatter than the first three response surfaces, and the variation of nanofiber diameter in both directions is small. From these plots, we can conclude

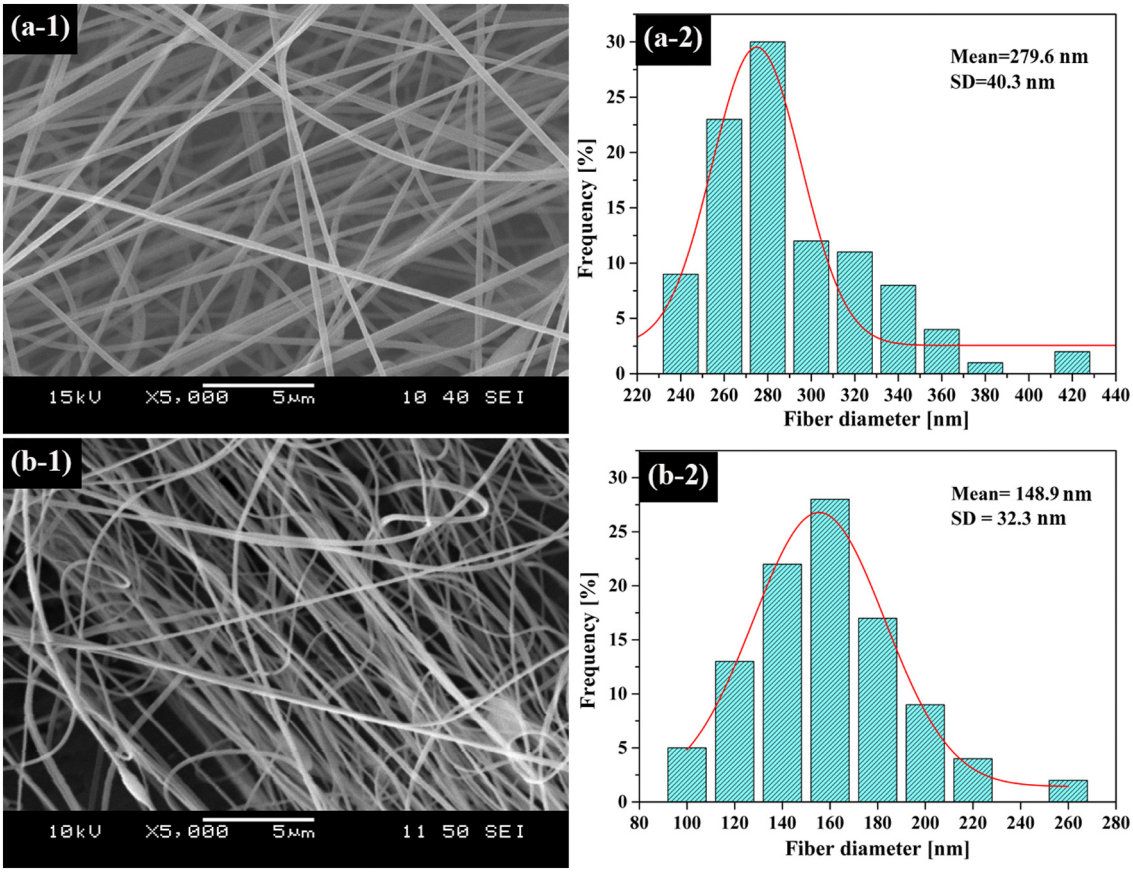

Fig. 3. SEM images and diameter distribution of nanofibers collected from (a) sample 2 and (b) sample 19.

Table 2
ANOVA table for average nanofiber diameter.

Source	Sum of squares	DF	Mean square	F-value	*p*-Value
Model	37,985	14	2713	38.20	<0.0001
X_1-Solution concentration	29,580	1	29,580	416.4	<0.0001
X_2-Collection distance	465.2	1	465.2	6.550	0.0227
X_3-Voltage	112.9	1	112.9	1.590	0.2281
X_4-Collection speed	12.47	1	12.47	0.1755	0.6816
X_1X_2	173.5	1	173.5	2.440	0.1405
X_1X_3	125.8	1	125.8	1.770	0.2045
X_1X_4	1.610	1	1.610	0.0227	0.8824
X_2X_3	132.9	1	132.9	1.870	0.1929
X_2X_4	24.03	1	24.03	0.3383	0.5700
X_3X_4	29.76	1	29.76	0.4189	0.5280
X_1^2	7228.45	1	7228.45	101.76	<0.0001
X_2^2	45.77	1	45.77	0.6444	0.4356
X_3^2	308.58	1	308.58	4.340	0.0559
X_4^2	256.55	1	256.55	3.610	0.0782
Error	994.50	14	71.040		
Total	38,979.83	28			

SD = 8.430.
R^2 = 97.45%.
Adjusted R^2 = 94.90%.
Predicted R^2 = 85.30%.

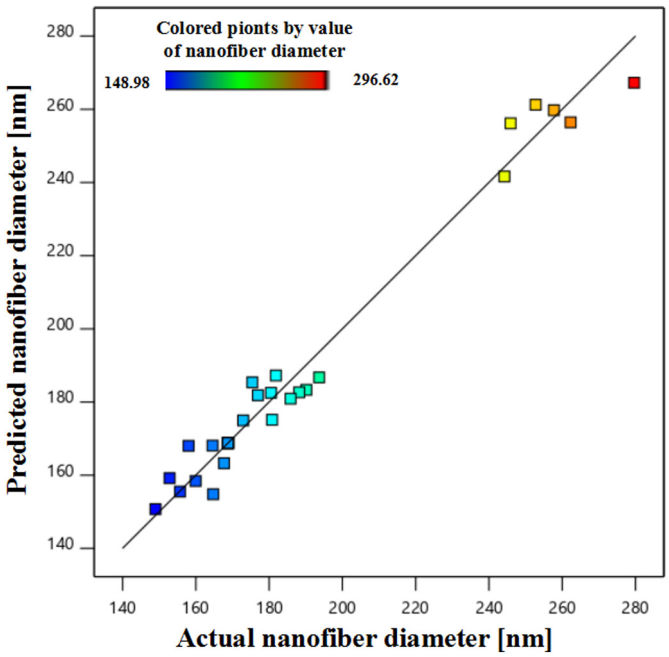

Fig. 4. Predicted nanofiber diameter *vs.* the actual nanofiber diameter.

that nanofiber diameter is not affected significantly by the interactions from collection distance, voltage, and collection speed.

Moreover, the contour curve at the bottom of each 3D surface response plot is a two-dimensional display of the surface response plot. It is a straightforward interpretation to locate optimum conditions for the best response if a maximum or minimum is regarded as the best response. It is desirable to make thinner nanofibers. When the contour plot has an always constant value in one direction (also called constant ridge) (see Fig. 6a, b, c), the optimum condition will be any point along

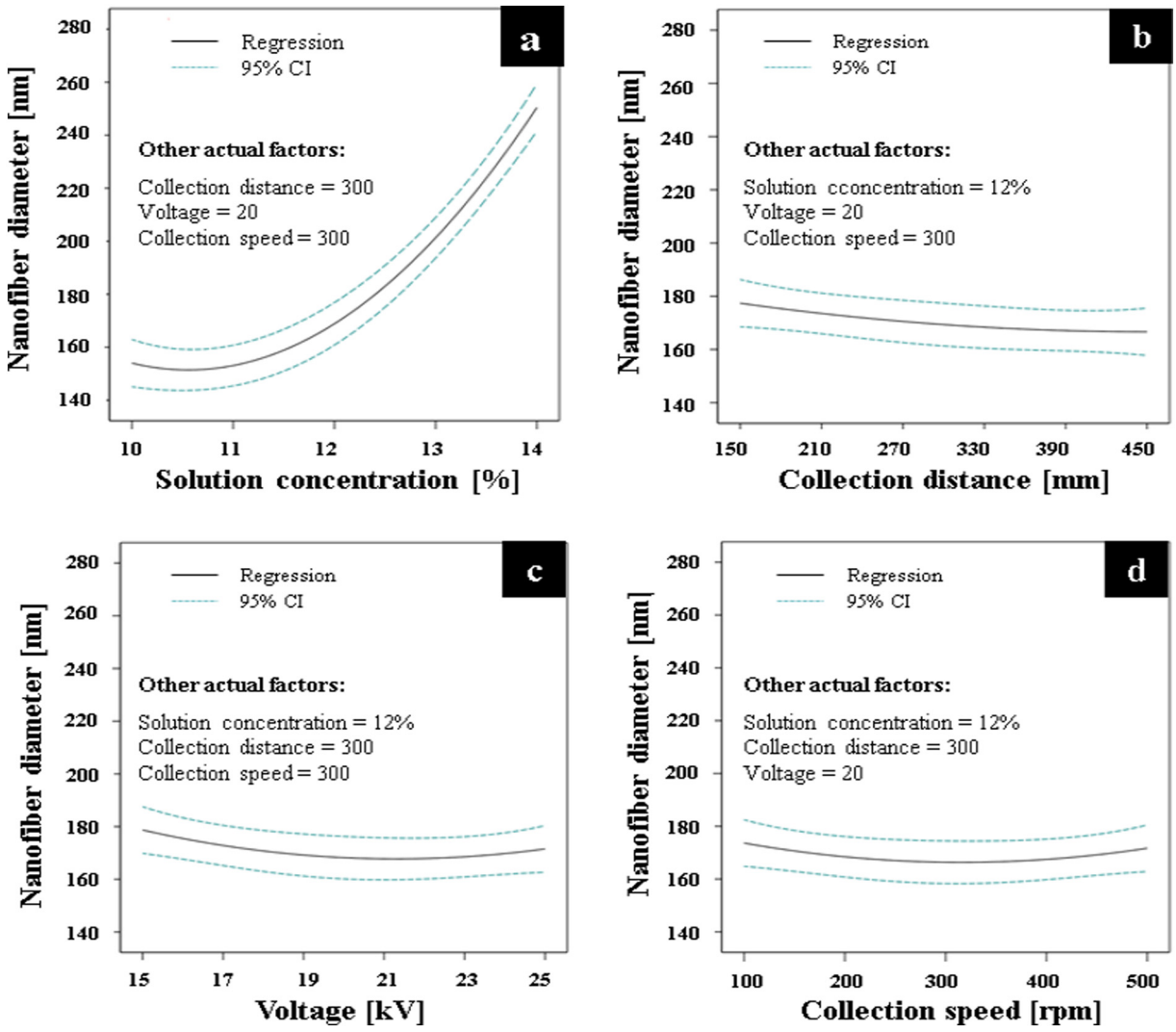

Fig. 5. The predicted relationship between single processing parameters and nanofiber diameter in the model: (a) solution concentration, (b) collector distance, (c) voltage, (d) collector rotation speed.

JMADE_108902-GR6.tif

Fig. 6. 3D response surface plots with different parameters for average fiber diameter: (a) solution concentration and collection distance, (b) solution concentration, and voltage, (c) solution concentration and collection speed, (d) collection distance and voltage, (e) collection distance and collection speed, (f) voltage and collection speed.

the ridge. When the contour curve is a rising ridge (see Fig. 6d, e), the optimum condition will be located at the vertex of the saddle curve. Furthermore, when the contour plot is a circle or ellipse (see Fig. 6f), there is a true optimum located at the center point of the contour plot. It will be a maximum or minimum, which is called a stationary point [44]. At this point, the slope in every direction is zero [45]. Therefore, the coordinates of the stationary point can be calculated when the first partial derivative is zero in the model. To simplify the analysis of experimental results, we only considered the essential terms within the empirical domain for optimum conditions. In the case of response in nanofiber diameter, there are no interaction terms included in the reduced model. Therefore, it can be directly concluded from the mathematical expression of the reduced model that the fiber diameter is mainly determined by the solution concentration (X_1). The thinnest nanofiber can be calculated with variable X_1 and fixed values of X_2 (300), X_3 (20), X_4 (300). Eventually, the optimum conditions to obtain the thinnest fibers (151.2 nm) are a solution concentration of 10.5%, a collection distance of 300 mm, a voltage of 20 kV and a collection speed of 300 rpm.

3.2. Correlation between processing parameters and fiber orientation

The best and worst orientated fibers were from samples 11 and 21, whose Herman's orientation factors were 0.336 and 0.087, respectively (Table S1). The SEM images and polar plot of fiber orientation from the two samples are shown in Fig. 7. There were a few beaded fibers in sample 11 because of the smallest solution concentration, but at the same time, the highest collection speed led to the best alignment of nanofibers. In contrast, the fibers from sample 21 with the slowest collection speed were less oriented. Compared with the polar plot of sample 21, the polar plot of sample 11 shows that fibers were distributed more narrowly and symmetrically in the collection direction.

Table 3 shows that the other three parameters (*i.e.*, collection distance, voltage, collecting speed), except solution concentration, show a significant effect on fiber orientation since their *p*-values are <0.05. The interaction of solution concentration and collection speed, collection distance, and voltage have a *p*-value <0.05, suggesting a significant

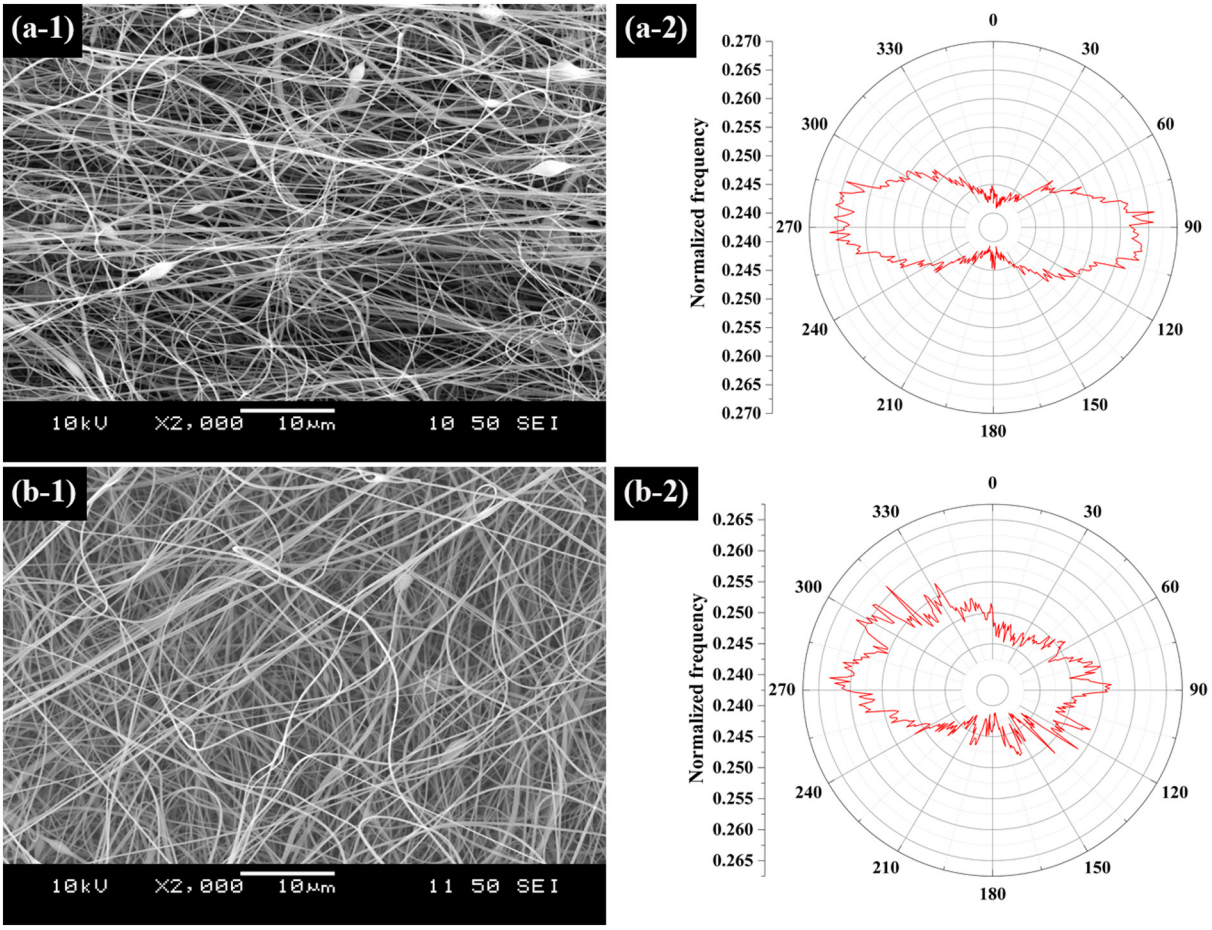

Fig. 7. SEM image and polar plot of fiber orientation collected from (a) sample 11 and (b) sample 21.

Table 3
ANOVA table for fiber orientation (Herman's factor).

Source	Sum of Squares	DF	Mean Square	F-value	*p*-Value
Model	0.1143	14	0.0082	16.34	<0.0001
X_1-Solution concentration	0.0011	1	0.0011	2.17	0.1630
X_2-Collection distance	0.0065	1	0.0065	12.99	0.0029
X_3-Voltage	0.0090	1	0.0090	18.06	0.0008
X_4-Collection speed	0.0608	1	0.0608	121.70	<0.0001
X_1X_2	0.0000034	1	3.486.250E−06	0.0125	0.9125
X_1X_3	0.0008	1	0.0008	1.630	0.2229
X_1X_4	0.0042	1	0.0042	8.460	0.0114
X_2X_3	0.0095	1	0.0095	19.040	0.0006
X_2X_4	0.0000	1	0.0000	0.0846	0.7754
X_3X_4	0.0011	1	0.0011	2.250	0.1561
X_1^2	0.0022	1	0.0022	4.310	0.0569
X_2^2	0.0191	1	0.0191	38.34	<0.0001
X_3^2	0.0037	1	0.0037	7.380	0.0167
X_4^2	0.0032	1	0.0032	6.410	0.0240
Error	0.0070	14	0.0050		
Total	0.1213	10			

Std. dev. = 2.230%.
R^2 = 94.23%.
Adjusted R^2 = 88.47%.
Predicted R^2 = 66.79%.

impact on fiber orientation. The *p*-value for the model is <0.0001, which indicates that the model is considered statistically significant. Moreover, the value of R^2 is 94.23% for the model, which shows that the model is in

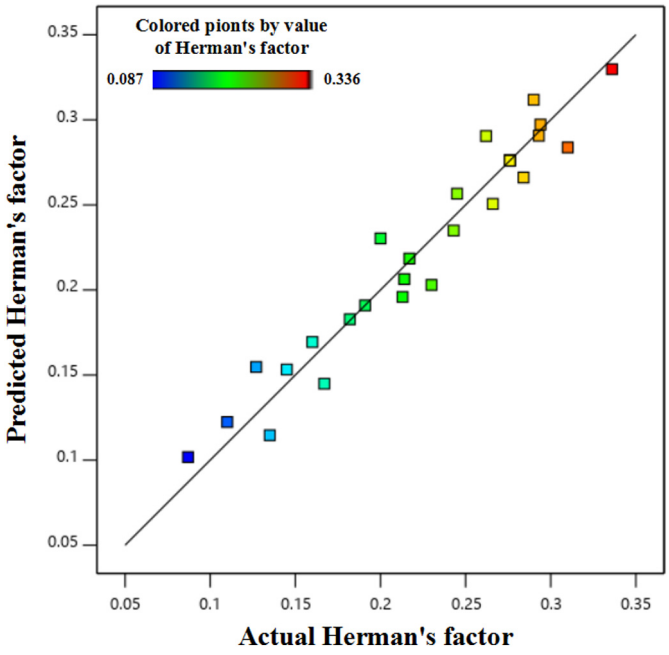

Fig. 8. Predicted Herman's factor and actual Herman's factor.

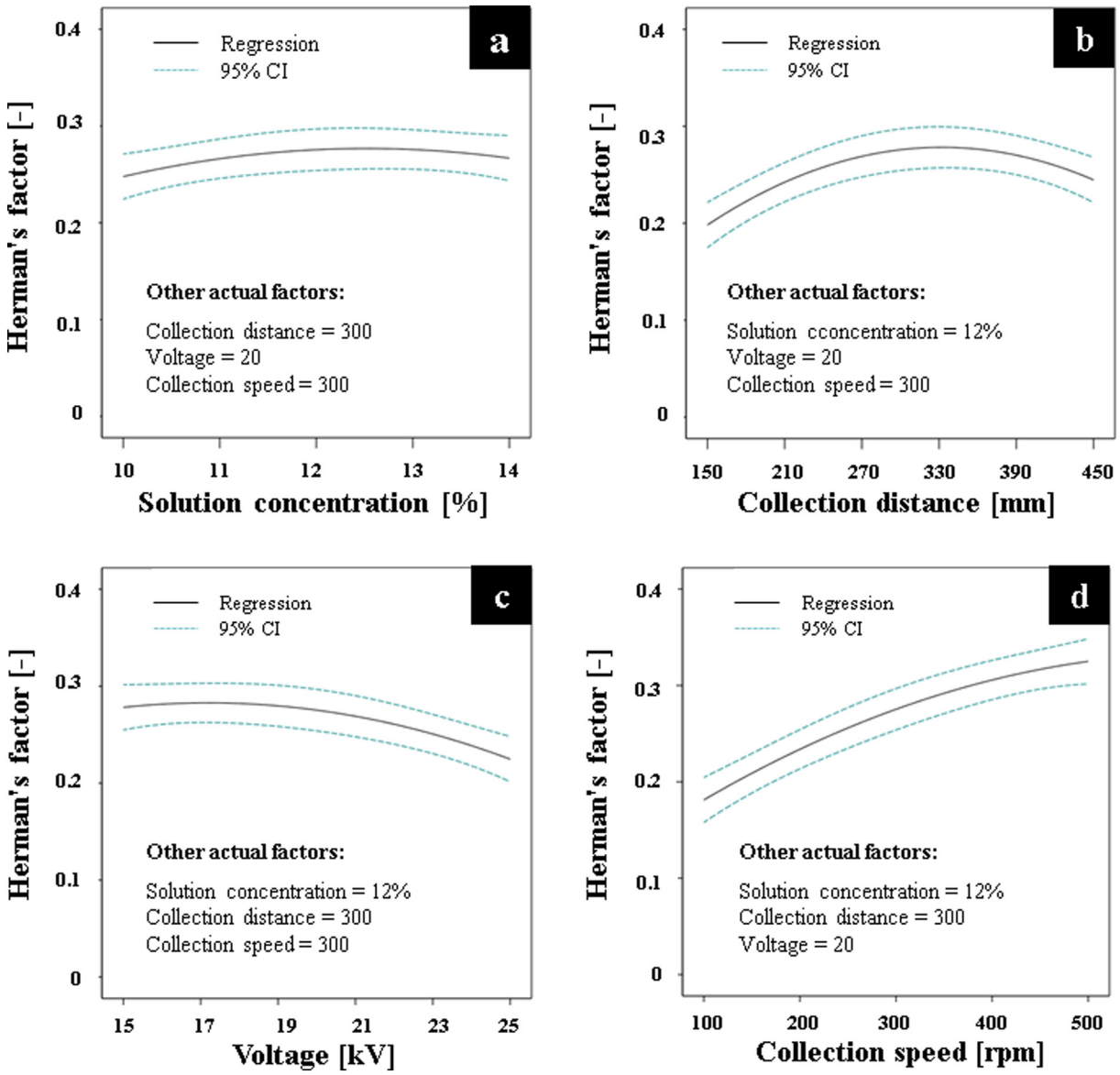

Fig. 9. The predicted relationship between a single processing parameter and Herman's factor in the model: (a) solution concentration, (b) collection distance, (c) voltage, (d) collection speed.

good agreement with experimental results. Also, the adjusted R^2 with a high value (88.47%) indicates that the model is applicable. The model obtained from ANOVA analysis can be written as shown in Eq. (4).

$$\begin{aligned} Y_2\ (\text{Herman's factor}) = {} & -1.39347 + 0.11125X_1 + 0.002986X_2 \\ & + 0.030025X_3 \\ & + 0.001361X_4 - 4.16667E-06X_1X_2 \\ & + 0.001425X_1X_3 - 0.000081X_1X_4 - 0.000065X_2X_3 \\ & - 1.08333E-07X_2X_4 \\ & + 0.000017X_3X_4 - 0.004552{X_1}^2 - 2.41481E \\ & - 06{X_2}^2 - 0.000953{X_3}^2 - 5.55208E-07{X_4}^2 \end{aligned} \quad (4)$$

The equation shows the relationship between processing parameters and fiber orientation. To simplify and further analyze the experimental results, we created a reduced model with only the significant terms to describe the variation in fiber orientation by the linear terms (X_2, X_3, X_4), interaction terms (X_1X_4, X_2X_3) and second-order term (X_2^2, X_3^2, X_4^2), as the other terms are not significant. Fig. 8 shows that the predicted fiber orientation has good agreement with the measured values, which suggests that the model was accurate.

The individual effect of solution concentration, collection distance, voltage, and collection speed on nanofiber orientation is shown in Fig. 9. Collection speed has the most significant effect among the four processing parameters because it caused considerable changes within the range of investigation. Nanofiber orientation increased with an increase in collection speed. It was because higher collection speed provided a more significant draw to improve the alignment of nanofibers [46]. In the experimental domain, the effect plot presents a monotonous increase, as shown in Fig. 9d. Additionally, we can also conclude that the effect of collection distance and voltage had more impact on fiber orientation, compared with solution concentration. With an increase in collection distance, the fiber orientation factor increased to a maximum and then decreased with even greater collection distances. When collection distance was small, two effects impaired the alignment of the fibers: (1) the velocity of fibers was higher when they arrived at the collector drum surface, and the velocity difference between the fibers and the drum was small, which could not provide a sufficient draw on the fibers; (2) when collection distance was small, there was no adequate stretching time before nanofibers were wound onto the collector.

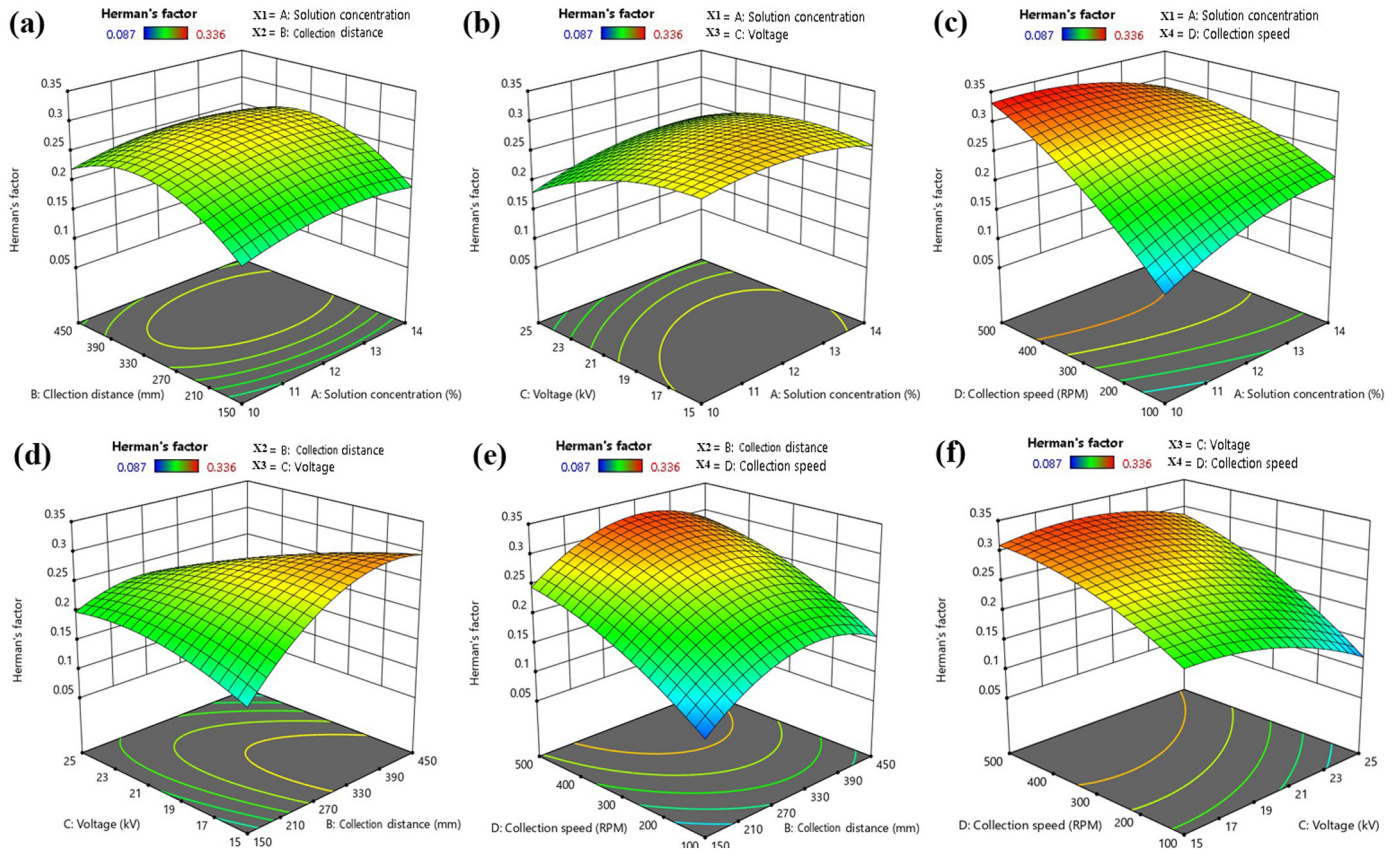

Fig. 10. 3D response surface plots with different parameters for fiber orientation: (a) solution concentration and collection distance, (b) solution concentration and voltage, (c) solution concentration and collection speed, (d) collection distance and voltage, (e) collection distance and collection speed, (f) voltage and collection speed.

Above the optimum collection distance, the reason for worsening fiber alignment was that from a long-distance, it became difficult to collect nanofibers in a single direction. That is because the electrical field between the nozzle and the collector was continuously changed, and the trajectory of fibers could not be kept stable over a longer collection distance. As voltage increased, the fibers became less oriented, which was the opposite tendency compared to DC electrospinning reported in the literature [47]. Hosseini et al. concluded that a higher voltage could accelerate the fiber to the collector, making it more challenging to alter the trajectory of the fiber [47]. On the other hand, in AC electrospinning, it is a different mechanism. Due to the fluctuating electrical field in the space between the nozzle and the collector, a higher AC voltage cannot accelerate the fibers continuously. However, it can generate more fibers with a bigger fibrous plume, resulting in difficult control over fiber trajectory. Compared to the three parameters mentioned above, solution concentration only had a minor effect on fiber orientation.

Fig. 10 shows the effect of the interaction of different parameters with 3D response surface plots that present the dependence of fiber orientation on two parameters within the experimental range. According to the interpretation of the contour plot in Section 3.1, we primarily analyzed the significant interaction terms (X_1X_4 and X_2X_3) for optimum conditions to achieve the highest Herman's orientation factor. Fig. 10c indicates that fiber orientation is highly dependent on collection speed, while solution concentration has little influence on it. The interactive effect of voltage and collection distance on nanofiber orientation is shown in Fig. 10d. Collection distance has more influence on nanofiber orientation than voltage. The contour plot also shows that nanofiber orientation improves with increasing voltage at shorter collection distances. At a longer collection distance, nanofiber orientation worsens. The contour plots in Fig. 10 c & d were rising ridges, and the optimum point should be located at one of the vertices along the ridge with the maximum. When the collection distance and voltage were set at 300 mm and 20 kV, respectively, the solution concentration and collection speed to obtain the most aligned nanofibers with a Herman's factor of 0.332 were 10.67% and 500 rpm.

3.3. Comparison of AC and DC electrospinning

Wei et al. [37] already investigated the influence of process parameters on the diameter of the nanofibers produced from DC electrospinning with the BBD model. Therefore, AC and DC electrospinning processes can be compared with respect to the effects of process parameters. In the literature, solution concentration had a significant influence on average fiber diameter. Obviously, in AC electrospinning, it was also found that solution concentration was the most significant factor affecting fiber diameter. A high-speed rotating drum collector increased fiber alignment [46,48] in DC electrospinning. In our study, we came to a similar conclusion; the rotation speed of the drum collector had a significant effect on fiber orientation. Therefore, solution concentration and collection speed play an equally important role in determining fiber diameter and orientation in both AC and DC electrospinning. However, the effect of voltage on fiber orientation has a different mechanism in AC electrospinning. In the DC electrospinning process, a higher voltage accelerates the jets and creates a more stable trajectory for them [47]. As a result, the fibers are deposited on the collector in a more oriented way. On the other hand, in AC electrospinning, due to the fluctuating electrical field in the space between the nozzle and the collector, a higher AC voltage cannot accelerate the fibers continuously. However, it can generate more fibers and form a bigger fiber column, resulting in problematic control of fiber trajectories.

4. Conclusion

AC electrospinning is a method that has great potential to produce nanofiber yarns because of its self-bundling behavior and multiple jets from a single droplet. We investigated the influence of the processing parameters of AC electrospinning on the morphology of nanofibers (*i.e.*, fiber diameter and orientation) using RSM. We used the BBD model to analyze and fiber diameter and orientation and predict them from solution concentration, collection distance, voltage, and collection speed. The results showed that solution concentration had a more significant effect on nanofiber diameter than voltage, collection distance, or collection speed. The average diameter of nanofibers increased with increasing solution concentration. Nanofiber orientation was mainly determined by collection speed. Higher collection speed provided more effective stretching, which improved the arrangement of nanofibers. In further research, we plan to focus on the molecular chain orientation of AC electrospun nanofibers and the fabrication of continuous AC nanofiber yarns.

Supplementary data to this article can be found online at https://doi.org/10.1016/j.matdes.2020.108902.

CRediT authorship contribution statement

Haijun He: Project administration, Funding acquisition, Conceptualization, Methodology, Investigation, Writing - original draft, Writing - review & editing.**Yimeng Wang:**Investigation, Validation.**Balazs Farkas:** Investigation.**Zsombor Kristof Nagy:**Writing - review & editing.**Kolos Molnar:**Project administration, Supervision, Funding acquisition, Conceptualization, Writing - review & editing.

Declaration of Competing Interest

The authors declare that they have no known competing financial interests or personal relationships that could have appeared to influence the work reported in this paper.

Acknowledgments

This work was supported by the BME-Nanonotechnology FIKP grant (BME FIKP-NAT), the Hungarian Research Fund (OTKA FK 131882), the ÚNKP-17-4-I New National Excellence Program of the Ministry of Human Capacities, the ÚNKP-19-4 New National Excellence Program of the Ministry for Innovation and Technology and BME-KKP. This paper was also supported by the János Bolyai Research Scholarship of the Hungarian Academy of Sciences (K. Molnár), Stipendium Hungaricum Scholarship of Tempus Public Foundation, and China Scholarship Council (201700500073).

References

[1] S.A. Theron, A.L. Yarin, E. Zussman, E. Kroll, Multiple jets in electrospinning: experiment and modeling, Polymer 46 (9) (2005) 2889–2899, https://doi.org/10.1016/j.polymer.2005.01.054.

[2] K. Wang, P. Wang, M. Wang, D.-G. Yu, F. Wan, S.W.A. Bligh, Comparative study of electrospun crystal-based and composite-based drug nano depots, Mater. Sci. Eng. C 113 (2020)https://doi.org/10.1016/j.msec.2020.110988.

[3] J. Yang, K. Wang, D.G. Yu, Y. Yang, S.W.A. Bligh, G.R. Williams, Electrospun Janus nanofibers loaded with a drug and inorganic nanoparticles as an effective antibacterial wound dressing, Mater. Sci. Eng. C Mater. Biol. Appl. 111 (2020), 110805. https://doi.org/10.1016/j.msec.2020.110805.

[4] M. Wang, K. Wang, Y. Yang, Y. Liu, D.G. Yu, Electrospun environment remediation nanofibers using unspinnable liquids as the sheath fluids: a review, Polymers (Basel) 12 (1) (2020)https://doi.org/10.3390/polym12010103.

[5] K. Wang, H.F. Wen, D.G. Yu, Y.Y. Yang, D.F. Zhang, Electrosprayed hydrophilic nanocomposites coated with shellac for colon-specific delayed drug delivery, Mater. Des. 143 (2018) 248–255, https://doi.org/10.1016/j.matdes.2018.02.016.

[6] D.G. Yu, M. Wang, X. Li, X. Liu, L.M. Zhu, S.W. Annie Bligh, Multifluid electrospinning for the generation of complex nanostructures, Wiley Interdiscip. Rev. Nanomed. Nanobiotechnol. 12 (3) (2020) e1601, https://doi.org/10.1002/wnan.1601.

[7] A. Mirek, P. Korycka, M. Grzeczkowicz, D. Lewińska, Polymer fibers electrospun using pulsed voltage, Mater. Des. 183 (2019)https://doi.org/10.1016/j.matdes.2019.108106.

[8] Y. Jin, Q. Gao, C. Xie, G. Li, J. Du, J. Fu, Y. He, Fabrication of heterogeneous scaffolds using melt electrospinning writing: design and optimization, Mater. Des. 185 (2020)https://doi.org/10.1016/j.matdes.2019.108274.

[9] J. Xue, T. Wu, Y. Dai, Y. Xia, Electrospinning and electrospun nanofibers: methods, materials, and applications, Chem. Rev. 119 (8) (2019) 5298–5415, https://doi.org/10.1021/acs.chemrev.8b00593.

[10] Y. Ding, H. Hou, Y. Zhao, Z. Zhu, H. Fong, Electrospun polyimide nanofibers and their applications, Prog. Polym. Sci. 61 (2016) 67–103, https://doi.org/10.1016/j.progpolymsci.2016.06.006.

[11] P. Vass, E. Hirsch, R. Koczian, B. Demuth, A. Farkas, C. Feher, E. Szabo, A. Nemeth, S.K. Andersen, T. Vigh, G. Verreck, I. Csontos, G. Marosi, Z.K. Nagy, Scaled-up production and tableting of grindable electrospun fibers containing a protein-type drug, Pharmaceutics 11 (7) (2019)https://doi.org/10.3390/pharmaceutics11070329.

[12] G. Duan, A. Greiner, Air-blowing-assisted coaxial electrospinning toward high productivity of core/sheath and hollow fibers, Macromol. Mater. Eng. 304 (5) (2019) https://doi.org/10.1002/mame.201800669.

[13] L. Yong, J.H. He, Bubble electrospinning for mass production of nanoflbers, Int. J. Nonlinear Sci. Numer. Simul. 8 (3) (2007) 393–396, https://doi.org/10.1515/IJNSNS.2007.8.3.393.

[14] T. Miloh, B. Spivak, A.L. Yarin, Needleless electrospinning: electrically driven instability and multiple jetting from the free surface of a spherical liquid layer, J. Appl. Phys. 106 (11) (2009)https://doi.org/10.1063/1.3264884.

[15] O. Jirsak, F. Sanetrnik, D. Lukas, V. Kotek, L. Martinova, J. Chaloupek, A Method of Nanofibers Production from a Polymer Solution Using Electrostatic Spinning and a Device for Carrying Out the Method, US, W02005024101, 2005.

[16] H. Niu, T. Lin, X. Wang, Needleless electrospinning. I. A comparison of cylinder and disk nozzles, J. Appl. Polym. Sci. 114 (6) (2009) 3524–3530, https://doi.org/10.1002/app.30891.

[17] K.M. Forward, G.C. Rutledge, Free surface electrospinning from a wire electrode, Chem. Eng. J. 183 (2012) 492–503, https://doi.org/10.1016/j.cej.2011.12.045.

[18] X. Wang, H. Niu, X. Wang, T. Lin, Needleless electrospinning of uniform nanofibers using spiral coil spinnerets, J. Nanomater. 2012 (2012) 1–9, https://doi.org/10.1155/2012/785920.

[19] X. Yan, J. Marini, R. Mulligan, A. Deleault, U. Sharma, M.P. Brenner, G.C. Rutledge, T. Freyman, Q.P. Pham, Slit-surface electrospinning: a novel process developed for high-throughput fabrication of core-sheath fibers, PLoS One 10 (5) (2015), e0125407. https://doi.org/10.1371/journal.pone.0125407.

[20] G. Yan, H. Niu, H. Shao, X. Zhao, H. Zhou, T. Lin, Curved convex slot: an effective needleless electrospinning spinneret, J. Mater. Sci. 52 (19) (2017) 11749–11758, https://doi.org/10.1007/s10853-017-1315-z.

[21] K. Molnar, Z.K. Nagy, Corona-electrospinning: needleless method for high-throughput continuous nanofiber production, Eur. Polym. J. 74 (2016) 279–286, https://doi.org/10.1016/j.eurpolymj.2015.11.028.

[22] L. Wei, R. Sun, C. Liu, J. Xiong, X. Qin, Mass production of nanofibers from needleless electrospinning by a novel annular spinneret, Mater. Des. 179 (2019)https://doi.org/10.1016/j.matdes.2019.107885.

[23] H. He, C. Liu, K. Molnar, A novel needleless electrospinning system using a moving conventional yarn as the spinneret, Fibers and Polymers 19 (7) (2018) 1472–1478, https://doi.org/10.1007/s12221-018-8183-2.

[24] H. He, Y. Kara, K. Molnár, In situ viscosity-controlled electrospinning with a low threshold voltage, Macromol. Mater. Eng. 304 (11) (2019), 1900349. https://doi.org/10.1002/mame.201900349.

[25] Y. Kara, H. He, K. Molnár, Shear-aided high-throughput electrospinning: a needleless method with enhanced jet formation, J. Appl. Polym. Sci. (2020) 49104, https://doi.org/10.1002/app.49104.

[26] P. Pokorny, E. Kostakova, F. Sanetrnik, P. Mikes, J. Chvojka, T. Kalous, M. Bilek, K. Pejchar, J. Valtera, D. Lukas, Effective AC needleless and collectorless electrospinning for yarn production, Phys. Chem. Chem. Phys. 16 (48) (2014) 26816–26822, https://doi.org/10.1039/c4cp04346d.

[27] A. Balogh, R. Cselko, B. Demuth, G. Verreck, J. Mensch, G. Marosi, Z.K. Nagy, Alternating current electrospinning for preparation of fibrous drug delivery systems, Int. J. Pharm. 495 (1) (2015) 75–80, https://doi.org/10.1016/j.ijpharm.2015.08.069.

[28] A. Balogh, B. Farkas, G. Verreck, J. Mensch, E. Borbas, B. Nagy, G. Marosi, Z.K. Nagy, AC and DC electrospinning of hydroxypropylmethylcellulose with polyethylene oxides as secondary polymer for improved drug dissolution, Int. J. Pharm. 505 (1–2) (2016) 159–166, https://doi.org/10.1016/j.ijpharm.2016.03.024.

[29] B. Farkas, A. Balogh, R. Cselko, K. Molnar, A. Farkas, E. Borbas, G. Marosi, Z.K. Nagy, Corona alternating current electrospinning: a combined approach for increasing the productivity of electrospinning, Int. J. Pharm. 561 (2019) 219–227, https://doi.org/10.1016/j.ijpharm.2019.03.005.

[30] C. Lawson, A. Stanishevsky, M. Sivan, P. Pokorny, D. Lukáš, Rapid fabrication of poly (ε-caprolactone) nanofibers using needleless alternating current electrospinning, J. Appl. Polym. Sci. 133 (13) (2016), 43232. https://doi.org/10.1002/app.43232.

[31] N. Naderi, F. Agend, R. Faridi-Majidi, N. Sharifi-Sanjani, M. Madani, Prediction of nanofiber diameter and optimization of electrospinning process via response surface methodology, J. Nanosci. Nanotechnol. 8 (5) (2008) 2509–2515, https://doi.org/10.1166/jnn.2008.536.

[32] T. Padmanabhan, V. Kamaraj, L. Magwood, B. Starly, Experimental investigation on the operating variables of a near-field electrospinning process via response surface methodology, J. Manuf. Process. 13 (2) (2011) 104–112, https://doi.org/10.1016/j.jmapro.2011.01.003.

[33] K. Nasouri, H. Bahrambeygi, A. Rabbi, A.M. Shoushtari, A. Kaflou, Modeling and optimization of electrospun PAN nanofiber diameter using response surface

methodology and artificial neural networks, J. Appl. Polym. Sci. 126 (1) (2012) 127–135, https://doi.org/10.1002/app.36726.
[34] P. Agarwal, P.K. Mishra, P. Srivastava, Statistical optimization of the electrospinning process for chitosan/polylactide nanofabrication using response surface methodology, J. Mater. Sci. 47 (10) (2012) 4262–4269, https://doi.org/10.1007/s10853-012-6276-7.
[35] M. Essalhi, M. Khayet, C. Cojocaru, G.-P. M.C. A.P., Response surface modeling and optimization of electrospun nanofiber membranes, Open Nanosci. J. 7 (2013) 8–17, https://doi.org/10.2174/1874140101307010008.
[36] H. Maleki, A.A. Gharehaghaji, G. Criscenti, L. Moroni, P.J. Dijkstra, The influence of process parameters on the properties of electrospun PLLA yarns studied by the response surface methodology, J. Appl. Polym. Sci. 132 (5) (2015), 41388. https://doi.org/10.1002/app.41388.
[37] L. Wei, Q. Qiu, R. Wang, X. Qin, Influence of the processing parameters on needleless electrospinning from double ring slits spinneret using response surface methodology, J. Appl. Polym. Sci. 135 (27) (2018), 46407. https://doi.org/10.1002/app.46407.
[38] S. Jiang, Y. Chen, G. Duan, C. Mei, A. Greiner, S. Agarwal, Electrospun nanofiber reinforced composites: a review, Polym. Chem. 9 (20) (2018) 2685–2720, https://doi.org/10.1039/c8py00378e.
[39] J.K. Alexander, B. Fuss, R.J. Colello, Electric field-induced astrocyte alignment directs neurite outgrowth, Neuron Glia Biol. 2 (2) (2006) 93–103, https://doi.org/10.1017/S1740925X0600010X.
[40] H. Zhang, H. Bai, S. Deng, Z. Liu, Q. Zhang, Q. Fu, Achieving all-polylactide fibers with significantly enhanced heat resistance and tensile strength via in situ formation of nanofibrilized stereocomplex polylactide, Polymer 166 (2019) 13–20, https://doi.org/10.1016/j.polymer.2019.01.040.
[41] M. Wang, T. Hai, Z. Feng, D.G. Yu, Y. Yang, S.A. Bligh, The relationships between the working fluids, process characteristics and products from the modified coaxial electrospinning of zein, Polymers (Basel) 11 (8) (2019)https://doi.org/10.3390/polym11081287.
[42] K. Zhao, W. Wang, Y. Yang, K. Wang, D.-G. Yu, From Taylor cone to solid nanofiber in tri-axial electrospinning: size relationships, Results in Physics 15 (2019)https://doi.org/10.1016/j.rinp.2019.102770.
[43] H. He, M. Gao, D. Torok, K. Molnar, Self-feeding electrospinning method based on the Weissenberg effect, Polymer 190 (2020), 122247. https://doi.org/10.1016/j.polymer.2020.122247.
[44] N. Sarlak, M.A.F. Nejad, S. Shakhesi, K. Shabani, Effects of electrospinning parameters on titanium dioxide nanofibers diameter and morphology: an investigation by Box–Wilson central composite design (CCD), Chem. Eng. J. 210 (2012) 410–416, https://doi.org/10.1016/j.cej.2012.08.087.
[45] R. Carlsson, Chapter 12 Response Surface Methods, Data Handling in Science and Technology, 8, 2005 249–324, https://doi.org/10.1016/s0922-3487(08)70259-4.
[46] M. Sadrjahani, S.A. Hoseini, V. Mottaghitalab, A.K. Haghi, Development and characterization of highly orientated PAN nanofiber, Braz. J. Chem. Eng. 27 (4) (2010) 583–589, https://doi.org/10.1590/S0104-66322010000400010.
[47] N. Shah Hosseini, B. Simon, T. Messaoud, N. Khenoussi, L. Schacher, D. Adolphe, Quantitative approaches of nanofibers organization for biomedical patterned nanofibrous scaffold by image analysis, J. Biomed. Mater. Res. A 106 (11) (2018) 2963–2972, https://doi.org/10.1002/jbm.a.36485.
[48] P. Nitti, N. Gallo, L. Natta, F. Scalera, B. Palazzo, A. Sannino, F. Gervaso, Influence of nanofiber orientation on morphological and mechanical properties of electrospun chitosan mats, J. Healthc. Eng. (2018) (2018) 3651480, https://doi.org/10.1155/2018/3651480.